Evaluation of new MR invisible silicon carbide based dielectric pads for 7 T MRI

Zo Raolison, Marc Dubois, Michel Luong, Ana Luisa Neves, Franck Mauconduit, Stefan Enoch, Nicolas Mallejac, Pierre Sabouroux, Fawzi Boumezbeur, Patrick Berthault, et al.

Version of Record: https://www.sciencedirect.com/science/article/pii/S0730725X22000558
Manuscript_4d9d0ffe82d54ccde01ae67a36863013

Title

Evaluation of new MR invisible silicon carbide based dielectric pads for 7T MRI.

Authors

Raolison, Zo[1,2]; Dubois, Marc[1,3,4]; Luong, Michel[2]; Neves, Ana Luisa[1,5]; Mauconduit, Franck[2]; Enoch, Stefan[3]; Mallejac, Nicolas[6]; Sabouroux, Pierre[3]; Boumezbeur, Fawzi[2]; Berthault, Patrick[7]; Zubkov, Mikhail[8]; Adenot-Engelvin, Anne-Lise[6]; Hertz-Pannier, Lucie[2]; Georget Elodie[1]; Abdeddaim, Redha[3]; Vignaud, Alexandre[2]

[1] Multiwave Imaging, Marseille, FR

[2] CEA NeuroSpin, DRF/Joliot/Neurospin, Université Paris-Saclay & CNRS, Gif-sur-Yvette, FR

[3] Aix Marseille Univ, CNRS, Centrale Marseille, Institut Fresnel, Institut Marseille Imaging, Marseille, France

[4] Aix Marseille Univ, CNRS, Centre de Résonance Magnétique Biologique et Médicale, Marseille, FR

[5] Assimilate, Marseille, FR

[6] CEA DAM Le Ripault, Monts, FR

[7] Université Paris-Saclay, CNRS, CEA, Nanosciences et Innovation pour les Matériaux, la Biomédecine et l'Énergie, Gif-sur-Yvette, FR

[8] Department of Physics and Engineering, ITMO University, Saint Petersburg, RU

Corresponding author

Alexandre Vignaud

CEA NeuroSpin, DRF/Joliot/Neurospin, Université Paris-Saclay & CNRS,

Centre d'études de Saclay, Bâtiment 145, 91191 Gif-sur-Yvette

Abstract

Purpose: The use of dielectric pads to redistribute the radiofrequency fields is currently a popular solution for 7T MRI practical applications, especially in brain imaging. In this work, we tackle several downsides of the previous generation of dielectric pads. This new silicon carbide recipe makes them MR invisible and greatly extends the performance lifespan.

Method: We produce a set of two 10x10x1cm^3 dielectric pads based on silicon carbide (SiC) powder dispersed in 4-Fluoro 1,3-dioxalan-2-one (FEC) and polyethylene Glycol (PEG). The stability of the complex permittivity and the invisibility of the pads are characterized experimentally. Numerical simulations are done to evaluate global and local SAR over the head in presence of the pads. B_0, B_1^+ and standard imaging sequences are performed on healthy volunteers.

Results: SiC pads are compared to state-of-the-art perovskite based dielectric pads with similar dielectric properties (barium titanate). Numerical simulations confirm that head and local SAR are similar. MRI measurements confirm that the pads do not induce susceptibility artefacts and improve B_1^+ amplitude in the temporal lobe regions by 25% on average.

Conclusion: We demonstrate the long-term performance and invisibility of these new pads in order to increase the contrast in the brain temporal lobes in a commercial 7T MRI head coil.

Keywords

Magnetic Resonance Imaging, Dielectric Materials, Ultra-High Field MRI, Radiofrequency Passive Shimming, SAR.

Introduction

With higher signal and contrast to noise ratio, ultra-high field magnetic resonance imaging (UHF MRI) provides unprecedented potential for clinical studies, neuroscientific research, and many other

applications. However, several limitations have been reported, hindering clinical application of UHF scanners. On one hand, static magnetic field (B_0) heterogeneities, induced inside the body at the interphases between regions with different magnetic susceptibilities, increase linearly with B_0 field intensity. It is harder and harder to correct them with classic second order shimming systems (1). They affect images, depending on the chosen sequences and contrasts, with distortions, hyposignals or hypersignals. In another hand, heterogeneous excitation of the nuclear spins represents another major issue at UHF. The phenomenon often called dielectric artefact involves constructive and destructive interference patterns related to the shortening of the RF wavelength used at these field strengths compared to the body part loading the coil (2, 3). It leads on the images to shadows or contrast losses across the imaged volume, making the affected regions diagnostically unexploitable (4). The correction of the latest is the topic of the work.

One simple way to address those inhomogeneities is to used pads containing High-Dielectric Constant (HDC) materials (relative permittivity >50), also called dielectric pads, inside a volume birdcage coil, classically used for radiofrequency (RF) transmission at UHF (5). Initially introduced by Foo et al. (6), the approach consists in taking advantage of the material high displacement currents to alter the global RF distribution from the transmit coil and generate a secondary localized RF field used to tune the B_1^+ field. HDCs were initially made of aqueous gels (7,8) or deionized water (9,10) to mimic the human brain permittivity. However, their use was cumbersome as they had to be sealed in rectangular bags filled by at least a few litres of liquid. Moreover, the advent of tight-fit receive array limited the available space around the patient.

A new generation of pads has been introduced based on perovskite compound mixed with water. It led to an increase in relative permittivity while reducing the size and thickness of the pads. Due to their properties, cost and availability, following studies focused on calcium titanate ($CaTiO_3$) (11,12). The relative permittivity achieved with this material was up to 120 depending on the volume fraction (13). Such levels of permittivity allowed improvement of transmit efficiency in temporal lobes (11) and cerebellum (14) regions of interest but required bulky pads with dimensions between 15 cm to 20 cm side

and thickness between 1 cm to 2 cm. Looking for further size and thickness reduction, barium titanate powders ($BaTiO_3$) were introduced, reaching relative permittivity up to 300 (13,15,16). Besides good performances, some drawbacks prevented their use in UHF clinical protocols: performance decay over time (16), reported toxicity and reduced patient's comfort (13). In such a composite material, high volume ratio of particles is needed to reach high levels of permittivity ($\varepsilon' > 200$) which was required to maintain high flexibility in the pad design. Since the water/titanate powder mixture reached saturation when powder volume ratio reaches around 45%, sedimentation appeared over time, reducing permittivity levels of the mixture after a few months. Moreover, starting at 40% powder volume ratio, pads had to be machine-pressed in order to reach the desired high level of permittivity. This resulted in uncomfortable rigid inserts that had to be set up between the coil and head of the patient. Compared to calcium titanate powders, barium titanate powders bear the toxicity rating "harmful if swallowed or inhaled" (17,18) which is a liability for any research centre or hospital striving for high level of human health and environment protections.

The pad degradation issue has been partially addressed by using dispersants in the mixture, which can expand lifespan by a few months, at the cost of higher imaginary part of permittivity ε'' and slightly lower performance (16). One remaining weakness of water-based perovskite pads was that they were visible on the MR images. Thus, heavy water (D_2O) was often used to make them invisible in MRI (3). Nevertheless, in addition to a large cost increase, the MR-invisibility induced this way tends to disappear over time (16). Despite these drawbacks, recent active studies established that dielectric pads remained a simple and popular solution for tackling RF inhomogeneities in clinical research (19).

The present work introduces an innovative alternative mixture to address limitations of perovskite-based pads. A low fusion temperature solvent combined with a safer dielectric material was compared to state-of-the-art $BaTiO_3$ water-based pads in order to assess its performances. Dielectric properties were measured over a year to determine its long-term performance. Specific Absorption Rate (SAR) simulations were performed for each configuration to demonstrate that this novel material can be safely

used in vivo for passive shimming. Finally, MRI in vivo study was conducted to assess the passive shimming performances.

Methods

HDC pad manufacturing

The specifications of the HDC pads used in this study have been chosen based on the results from a previous work (20). Criteria include the highest local B_1^+ local enhancement in both temporal lobes and a constant 1 cm thickness to fit inside the coil with most of the volunteer head sizes. Numerous HDC surfaces and properties (e.g. ε' and ε") were simulated which results converged to an optimal values of 10 x 10 cm² pads with ε'>250 and ε"~50. A more systematic solution to optimize the HDC pad specifications, such as the one proposed in (21), was not considered in this work because it only allowed targeting a single region where B_1^+ had to be enhanced.

SiC pads were fabricated from silicon carbide (SiC) spherical particles (Neyco, Vanves, France) mixed with solvent 4-Fluoro 1,3-dioxalan-2-one (FEC) (Chemos, Regenstauf, Germany) with a powder volume ratio of 69%. Particles were -1250 mesh (10 µm). Polyethylene glycol (PEG) (Sigma-Aldrich, Saint Louis, USA) was added as dispersant agent (1% of total weight) for the slurry homogeneity. The mixtures with increasing quantity of SiC powder were prepared and characterized until reaching the target values. A multiple phase Lichtenecker's logarithmic power law (22) was used to help predict the results. The mixture exhibiting highest permittivity and lowest conductivity was used for the performance study presented in the article (23).

$BaTiO_3$ pads were fabricated from barium titanate powder (Alfa Aesar, Averhill, USA) mixed with deuterated water (Sigma-Aldrich, Saint Louis, USA) with a powder volume ratio of 83%. Particles were -325 mesh (44 µm).

$BaTiO_3$ and SiC composites were sealed into 160 µm thick double layer Polypropylene-Polyamide standard pouches with a Lava V400 Sealer (Lava, Bad Saulgau, Germany). Pouches sizes are 10.0×10.0 ×1.0 cm^3 after sealing.

SiC mixture characterizations

We measured the T_2 and T_2* of the SiC material in a 7T NMR (Bruker, Ettlingen, Germany) with non-selective MR spectroscopic Multi-Spin-Multi-Echo (MSME) (7×TE with ΔTE 5.2ms) and Free Induction Decay (FID) sequences correspondingly. Parameters were extracted using mono-exponential fitting for T_2 and using Lorentzian-fitting directly on the FFT of the signal searching for Full Width at Half Maximum (FWHM). Characterization of the complex permittivity of the mixture were carried out through Nicolson and Ross protocol combined with a de-embedding process using a coaxial cell, sample holder and an in-house developed setup (24,25). Complex permittivity characterizations were performed at t = 0 months, 6 months, 9 months, and 12 months. Between each measurement, the sample was stored in a fridge at 5°C. The accuracies of the relative permittivity measurements are +/- 5% for the real part and +/- 10% for the imaginary part.

SAR simulations

Before carrying out in vivo measurements, and to ensure the absence of electric field hotspots, a preliminary evaluation was performed to provide SAR estimations. We used the time domain solver of CST Studio Suite (Dassault Systèmes, FR). Gustav voxel data (Adult, male) was truncated at the neck level and imported in the coil (16 legs high pass standard head birdcage). It included eleven different tissue materials. An anisotropic grid containing 1.5 million cells was applied with open boundary conditions. The criteria convergency was set at -50 dB. Similar simulation settings were used in the literature (26). SAR was calculated at 298 MHz with the IEEE/IEC 62704-1 averaging method implemented in the software. Two pads were introduced on both ears. Pad dimensions were 10.0×10.0×1.0 cm^3. Electromagnetic properties for SiC pads and $BaTiO_3$ pads were respectively $\varepsilon'=270$; $\varepsilon''=70$ ($\sigma=1.17$ S/m) and $\varepsilon'=340$; $\varepsilon''=30$ ($\sigma=0.50$ S/m). The pads were aligned at the ears level. For the simulation, we used a shielded high-pass birdcage coil with 5.2 pF capacitors and 16 rungs of 1 cm width and 22 cm height. The shield diameter was 31 cm and the birdcage inner diameter was 26 cm. The simulated birdcage has been

designed to mimic the transmission head birdcage used in our MR system and to resonate, when loaded, at 298 MHz which is the Larmor frequency of our 7T scanner with reflection amplitude below -14 dB. Simulations were done without additional tuning or matching circuits. In this case, head SAR corresponds to the SAR averaging over the whole head mass, and the maximal local SAR corresponds to the maximum value of local RF exposure, averaged over 10 grams of tissue (27) for an accepted power of 1 W and for a magnetic field flux density (B_1^+ amplitude) of 1 μT in the middle of the brain.

SAR values were evaluated on the whole head model and normalized to i) the coil accepted power and ii) the amplitude of the magnetic field flux in the middle of the brain. B_1^+ amplitude was presented as averaged in each ROI and compared relatively to the reference case for each volunteer. The percentage of enhancement was later averaged across the sample size.

In vivo MRI measurements

MRI experiments have been carried on 7T Magnetom MRI scanner (Siemens Healthineers, Erlangen, Germany) with a 1Tx/32Rx head coil (Nova Medical, Willington, MA, USA). Taking into account the strong local effect expected, the statistical power calculation indicated that a small number of volunteers was required to demonstrate the benefit. A first set of in vivo measurements was conducted on 4 healthy volunteers (1 Male and 3 Females aging between 19 and 21 years old) under “restricted SAR mode” constraints (24) with and without each set of pads for validation purpose. Once a good confidence was achieved with measurements in good agreement with the simulations, another set of in vivo measurements was conducted to obtain high resolution anatomical images with and without SiC pads under Normal SAR constraints. Studies were approved by the local and national ethics committees (CPP Sud Méditerranée 4, number 18 09 13, IDRCB: 2018-A011761-53) and (CPP Ile-de France 8, number 16 11 76 IDRCB 2016-AO1725-46) respectively. All volunteers gave a written informed consent.

In vivo preliminary acquisitions

To ensure volunteer safety during preliminary experiments, we adopted a very conservative strategy regarding RF exposure. Following Vignaud et al (28), the constraint set relied simply on energy conservation to guarantee the respect of the IEC guidelines: even if, hypothetically, the total input RF power was focused in a single 10g-piece of biological tissue, regulatory SAR limits would not be exceeded. An additional 2.5mm isotropic B_0 map which respects the same restricted SAR mode has been acquired on one of the volunteers to assess the influence of the presence of the HDC pads on magnetic field homogeneity. The sequence was a 3-echoes 3D gradient recalled echo sequence acquired in sagittal view with the following parameters: FOV=256×200×160mm^3, matrix 128×100×64, Bw=1085Hz/px, TE1/TE2/TE3/TR= 1.11/2.89/4.67/164ms, TA 9min54s. Each sequence respects the above-mentioned criterion and delivers valuable MR images in a reasonable acquisition time (TA). Measurements were done with and without the SiC and $BaTiO_3$ pad couples described above. Local B_1^+ field improvements were quantified on several healthy volunteers to assess reproducibility of the findings. The relative B_1^+ enhancement was specifically assessed in ROI located in regions known to be strongly affected by RF heterogeneities (e.g. temporal lobes).

High resolution in vivo acquisitions

A full MR protocol was acquired on a single healthy female participating as a control subject in a young adult Temporal Lobe Epilepsy (TLE) clinical study. A multi-slice T_2 weighted Turbo Spin-Echo (TSE) sequence was acquired in coronal view focusing on the hippocampus. Three interleaved stacks of 22 slices of 1.2mm were acquired to achieve a continuous slab (29) and a FOV of 192 ×192mm² (768×768 matrix) to obtain an in-plane resolution of 0.25mm². Relaxation parameters were TR/TE=6000/57ms, with hyper echo ETL (echo train length) = 9 and 120° refocused pulse. The Bandwidth was Bw = 171Hz/pixel, the acceleration factor R=2 with a GRAPPA reconstruction, with one average, for a total of TA = 12min30s. In this case, the acquisitions were done under IEC Normal SAR limitations.

Results

SiC mixture characterizations

Figure 1 presents T_2* and T_2 relaxation times respectively measured using the FWHM of the FID and MSME signal decay. The T_2* value was evaluated to 0.19 ms (+/- 0.02 ms) and the T_2 value was evaluated to 6.63 ms (+/- 0.15 ms) with a mono exponential fit.

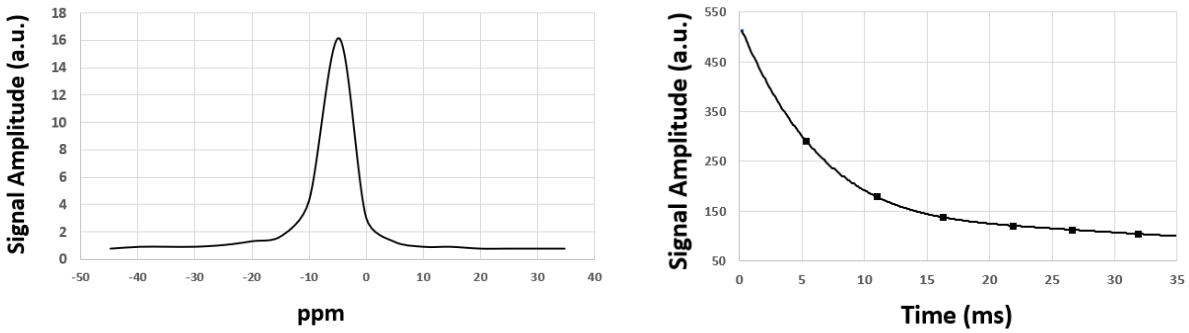

Figure 1: *On left plot, SiC mixture amplitude spectrum at 7T. FWHM* $\Delta\nu = 1/\pi T_2^* = 1700$ *Hz leading to* $T_2^* = 0.19$*ms. On the right plot, same mixture analyzed with MSME leading to very short relaxation time of* $T_2 = 6.6$*ms.*

We characterized the dielectric properties of the SiC mixtures over a one-year period. The results in terms of real part and imaginary part of the permittivity are presented in Figure 2. We observed an increase of +4 to +5% on the real part of the permittivity and +5 to +8% on the imaginary part. These changes lie within the uncertainty of the measurement technique used.

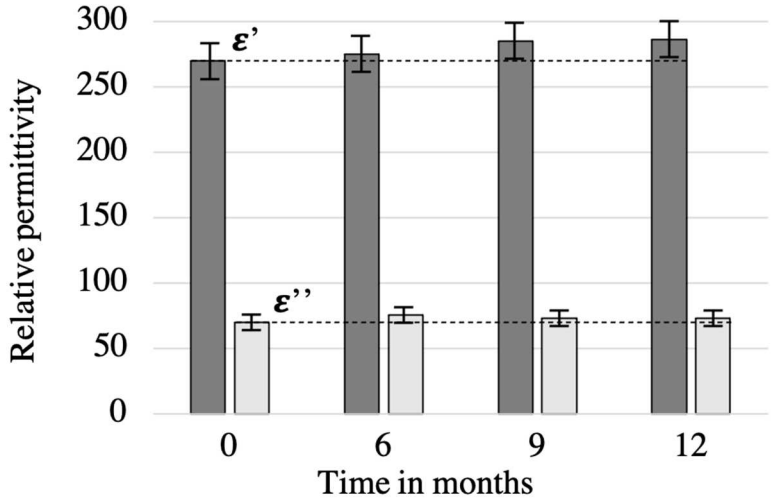

Figure 2: *Complex permittivity measurement for the SiC mixture over a one-year period. Real part (dark gray) and imaginary part (light gray) of the relative permittivity are presented.*

SAR simulations on voxel model

Local SAR_{10g} distributions were computed in CST Studio Suite using "Gustav" voxel model in a shielded birdcage without and with SiC and $BaTiO_3$ pads located on both ears. Three orthogonal views are displayed in Figure 3 and the quantitative analysis of head SAR and maximum local SAR are provided in Table 1. We observed that results normalized to accepted power present a reduction of head SAR and maximum local SAR of a few percent. When normalized to the magnetic field flux in the centre of the brain, the head SAR levels from each simulation become higher than the reference case by 4% for the barium titanate and by 2% for the silicon carbide pads. The local SAR levels tend to increase as well but stayed below the reference value again by 4% for the barium titanate and by 1% for the silicon carbide pads.

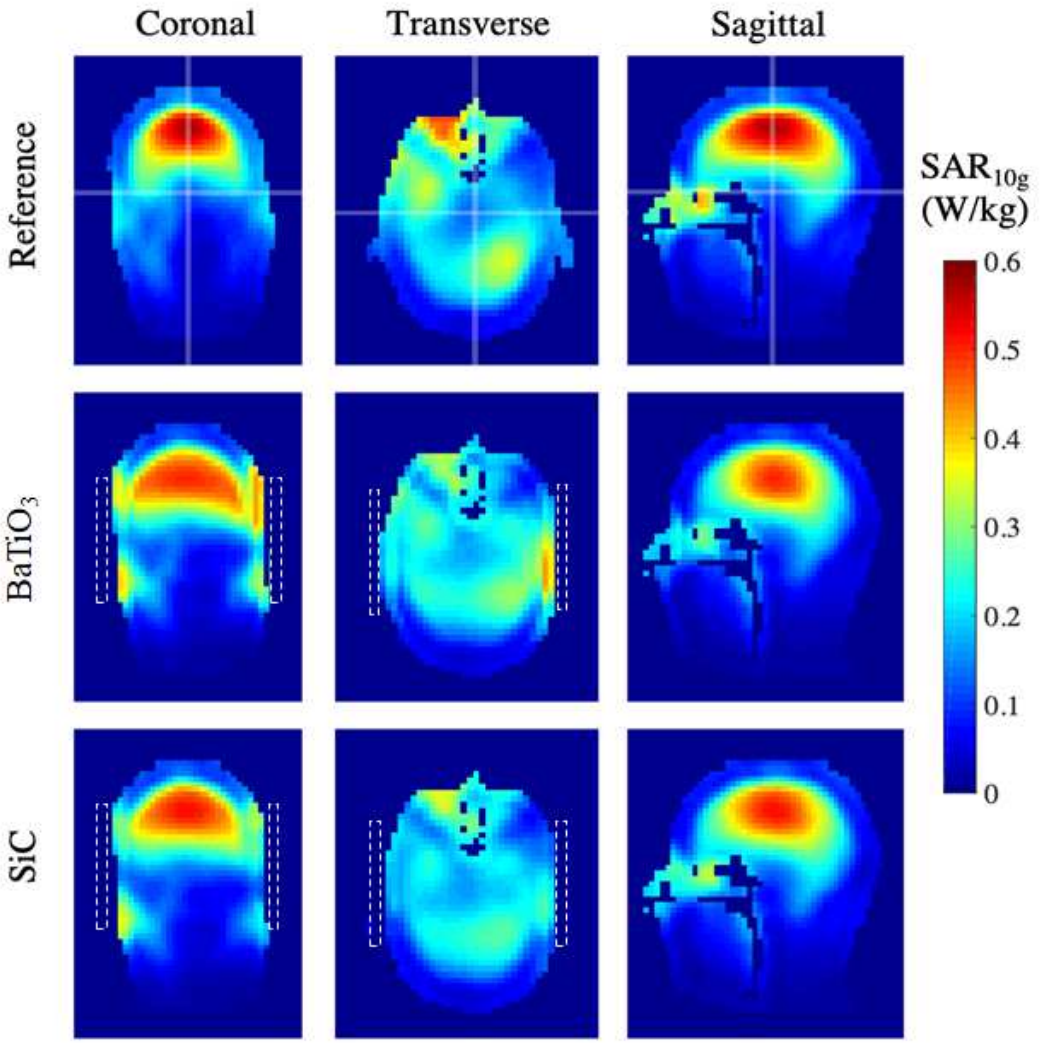

Figure 3: *Local SAR_{10g} maps in three orthogonal slices using Gustav head model. Reference is shown in the top row, the central row presents the results for two $BaTiO_3$ pads, the lower one shows results for two SiC pads. Simulation results are normalized to 1 W accepted power. The relative positions of the slices are depicted in transparency in the first row. Dotted white rectangles on coronal and transversal views represented dielectric pad positions for the simulation. In comparison with the reference, the local SAR increased in regions near the pads such as ears and lower on the neck. Nevertheless, the maximum local SAR, that is the key element for patient safety, remained located in the middle of the brain and was almost unaffected (see Table 1).*

Table 1: *SAR values obtained for the different simulated cases. Head (global) SAR and maximum local SAR are normalized for an accepted power of 1W and for a B_1^+ amplitude of 1µT of magnetic field flux in the middle of the brain.*

	Normalized to 1W accepted		**Normalized to 1µT in the middle of the brain**	
	Head SAR in W/kg	Max local SAR_{10g} in W/kg	Head SAR in W/kg	Max local SAR_{10g} in W/kg
Reference	0.145	0.571	0.164	0.645
$BaTiO_3$	0.141 (-2.8%)	0.506 (-11%)	0.170 (+4%)	0.622 (-4%)
SiC	0.138 (-5%)	0.519 (-9%)	0.167 (+2%)	0.638 (-1%)

In vivo MRI acquisitions

B_1^+ amplitude maps obtained in the restricted SAR protocol are shown on volunteer #1 in Figure 4a for two slice orientations. The coronal slice shows a good improvement of B_1^+ amplitude in the lower part of the temporal lobes which will be used for quantification. From the transverse orientation, we can see that the improvement is not constant across the brain volume. B_1^+ amplitude in the temporal lobe located on the right of the images is improved homogeneously by each set of pads. However, the homogeneity on the left side is not as good for each set of pads. It has also to be noted that SiC solvents (FEC ($C_3H_3FO_3$) and PEG ($C_2H_{4+2}O_1$) products) includes hydrogen bonds. Consequently, they are prone to resonate and produce sporadic chemical shift artefacts if present in a quantity large enough to be detectable during MR acquisition which is apparently not the case.

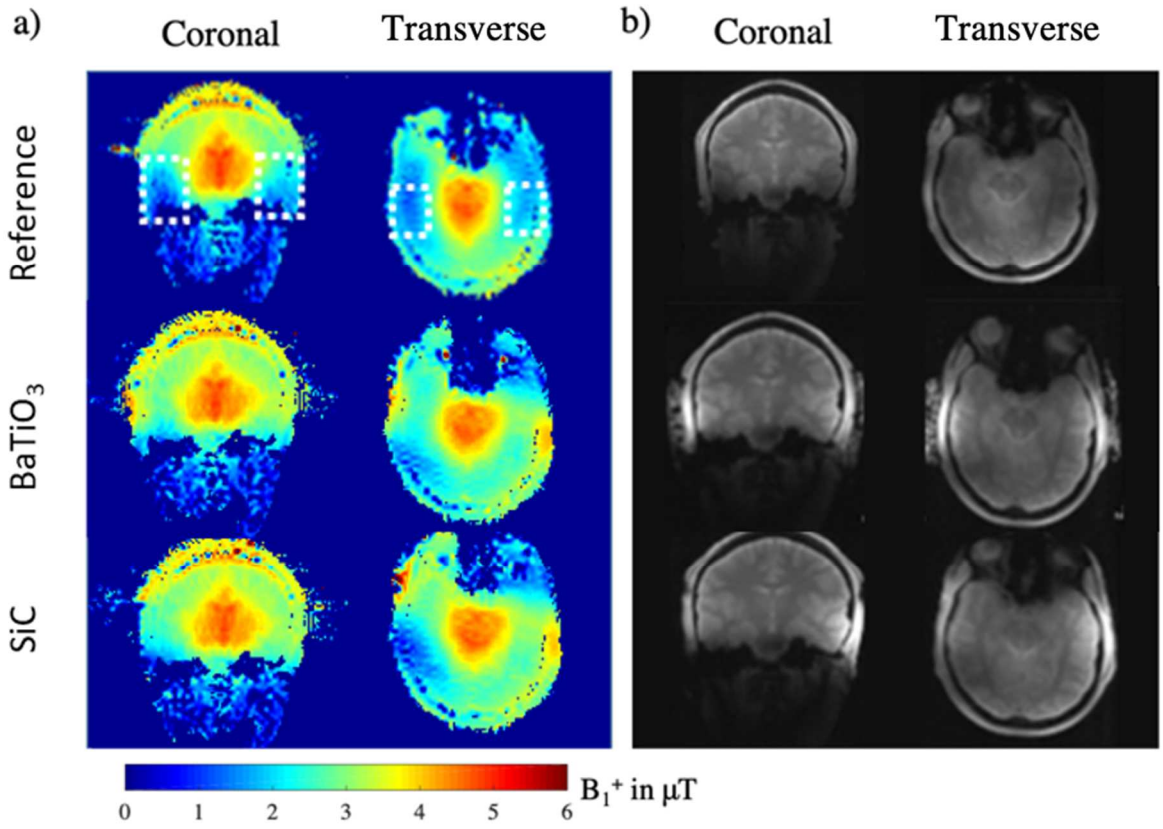

Figure 4: *a) B_1^+ amplitude maps on volunteer #1 in restricted mode (coronal view on left and transverse view on right). On top row, the reference measurement without pads, with two $BaTiO_3$ pads on second row, and two SiC pads on the last row. Regions of interest (ROIs) are presented in white dashed rectangle in the first row. Observed field increases are reported in Table 2. b) Proton Density (PD) images acquired at 7T on volunteer #1 in restricted mode (coronal view on left and transverse view on right). On top row, the reference measurement without pads, with two $BaTiO_3$ pads on second row, and two SiC pads on the last row. Brain images exhibit overall better intensity in the temporal lobes while pads are used. It can be noted that $BaTiO_3$ pads are visible in the second raw due to aging (over 6 months).*

Table 2 presents the results of the B_1^+ field enhancement with the pad obtained for the four volunteers. B_1^+ amplitude in the temporal lobes is increased on average by 29% in the case of $BaTiO_3$ pads and to 25% in the case of the SiC pads. Head diameter was smaller for the female volunteers (#2 #3 and #4) which results in higher B_1^+ amplitude in the reference maps for these cases. Consequently, the enhancements shown in

the Table 2 are reduced but the pads were still able to improve the transmit coil performance in the temporal lobes.

Table 2: *Values of B_1^+ Normalized Root Mean Square Error (NMRSE) (%) and B_1^+ field enhancement (%) between the reference case and the cases with pads in regions of interest (ROIs) located close to the pads in the temporal lobes for the four volunteers are displayed for coronal and transversal views. ROIs locations are depicted in white dashed rectangles in the Figure 4a.*

		Volunteer	**#1**	**#2**	**#3**	**#4**	**Average**
Reference	Coronal	B_1^+ NMRSE	38	33	44	36	**42**
	Transverse		52	32	68	32	**37**
$BaTiO_3$	Coronal	B_1^+ NMRSE	28	28	39	31	**30**
		B_1^+ local enhancement	+46.6	+31.9	+21.8	+28.3	**+30.1**
	Transverse	B_1^+ NMRSE	40	33	63	30	**38**
		B_1^+ local enhancement	+46.9	+23.0	+22.0	+30.8	**+26.9**
SiC	Coronal	B_1^+ NMRSE	25	25	41	26	**28**
		B_1^+ local enhancement	+31.5	+24.2	+12.0	+25.2	**+24.7**
	Transverse	B_1^+ NMRSE	37	37	70	31	**40**

B_1^+ local enhancement	+34.4	+28.0	+17.0	+22.1	**+25.0**

On average the SiC pads provided an B_1^+ amplitude enhancement of +25% in the temporal lobe ROIs with respect to the reference case. This enhancement was evaluated to be 3 to 4% less than with the $BaTiO_3$ pads. Obtained low spatial resolution proton density weighted brain images are presented in the Figure 4b for the same volunteer. They lead to enhanced contrast in the temporal lobes on the brain image, especially visible on the coronal view. High signal intensity spots are visible close to the pads' location due to high B_1^+ amplitude near the pads. It must also be noted that due to the aging of the $BaTiO_3$ pads (6 months), they can be detected. On the other hand, same age SiC based pads remained invisible on the image. Normalized Root Mean Square Errors (NRMSE) calculated over the whole brain section on the coronal and the transversal slices stayed very high with or without dielectric pads. The values ranged from 32 to 68% without pads and from 25 to 70% with pads depending on the slice orientation and volunteer. At an individual level, B_1^+ NRMSE is only slightly modified by the dielectric pads (within +/- 6% deviation).

We investigate potential magnetic susceptibility effects of the dielectric pads. We acquired frequency maps with and without each set of dielectric pads on one healthy volunteer after standard shimming procedure. Figure 5 presents the results in coronal and transverse slices. The results confirm the limited influence of HDC pads on the B_0 maps after standard shimming procedure.

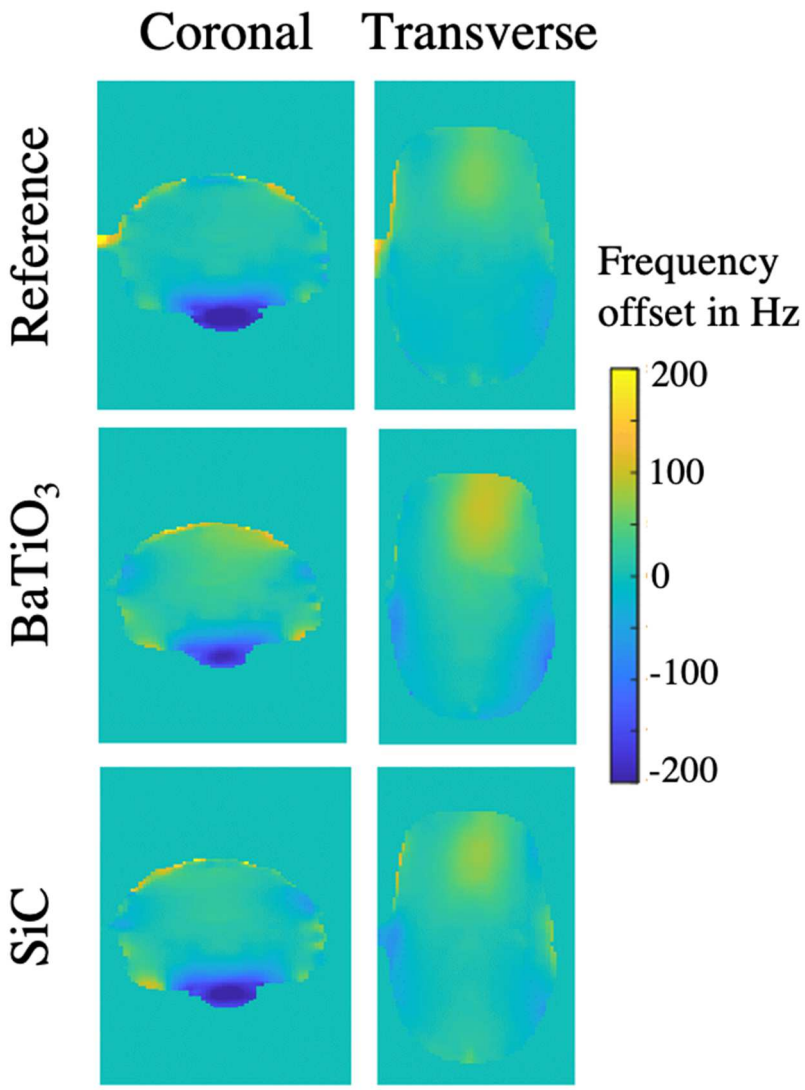

Figure 5: *Coronal and transverse masked field-map (Hz) views obtained on a healthy volunteer without pad (Reference), $BaTiO_3$ pads, then SiC pads, acquired with a 3-echoes 3D GRE sequence, in restricted SAR mode, at an $(2.5mm)^3$ isotropic spatial resolution after 2 iterations of B_0 shimming procedure.*

High spatial resolution T_2 weighted brain images, acquired under classic SAR constraints, are shown along coronal and transverse orientations for one volunteer in the Figure 6. The SiC pads remained invisible and delivered enhancement in the temporal lobe regions as expected. The signal and contrast gain after the positioning of the pads are sizable.

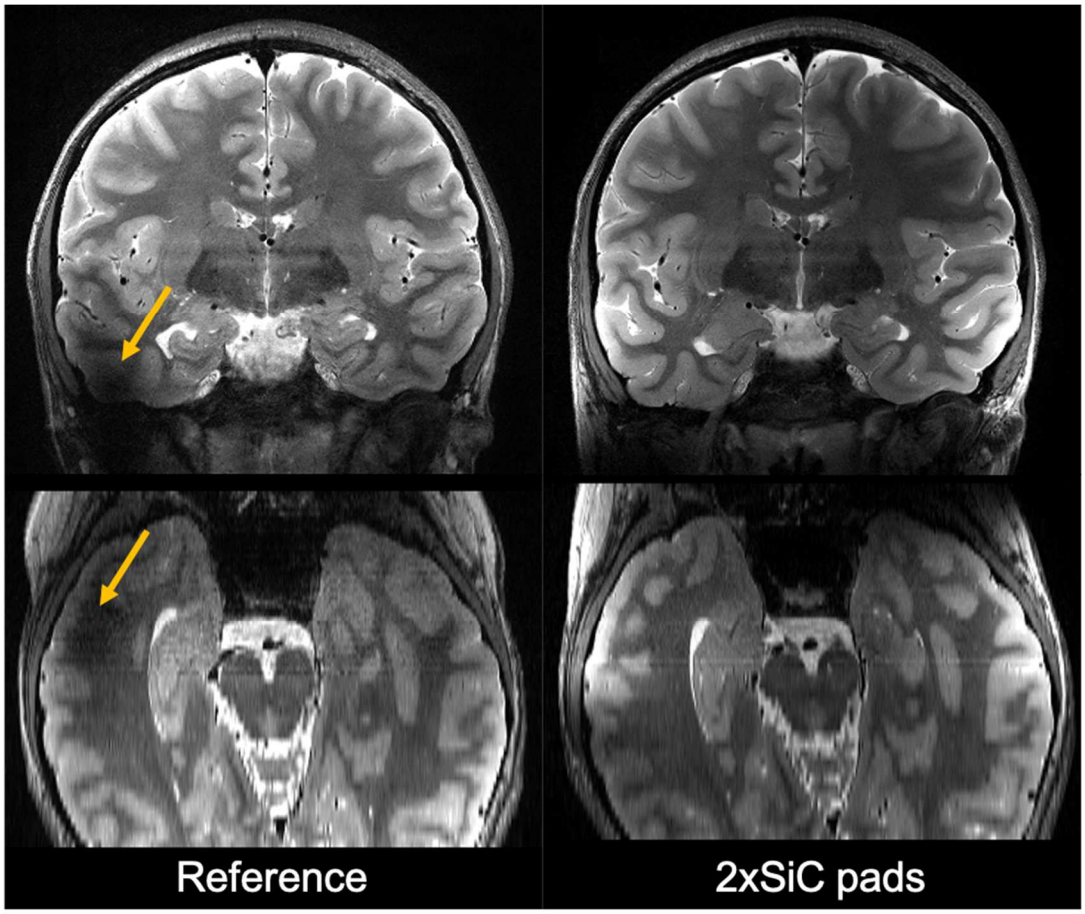

Figure 6*: High resolution 2D T2 weighted images acquired at 7T on one healthy volunteer with and without SiC pads and a 1Tx/32Rx head coil. The upper images show a coronal slice (250µm in plane resolution) of the reference scan without pads on the left. On the right, the same slice location with two SiC pads facing both ears is presented. Below reconstructed T2 weighted transverse images of the same data set (anisotropic pixel size) to show how large the SiC pad effect is are presented. It is particularly striking on the right temporal lobe (orange arrows on the left side of the images). Brain images exhibit overall stronger intensity and contrast close to the pads while they are used. No filter was applied on the images. Images were scaled differently to better depict the contrast improvement obtained with the SiC pads in the brain temporal lobes. We can also make the emphasis on the invisibility of the pads on the MR images.*

Discussion

Recent active studies established that dielectric pads remained the most popular solution available for tackling RF inhomogeneities in clinical research (19). Simultaneously, sizes and shapes have also been widely studied aiming to enhance their performance (15, 16, 20, 21). Additional simulations demonstrated that pads can be combined with metasurfaces to further enhance their performance. As an example, pads were enhanced by coupling with metasurfaces (30) or even by using a particular a fractal geometry (31) in order to combine their secondary generated field with the metasurface resonances. Our goal was to propose an alternative composition for dielectric pads that solved some of the limitations of barium titanate mixtures used in pads with very high permittivity $\varepsilon' > 200$. Our objectives were to (i) maintain safety rating of the dielectric slurry, (ii) ensure invisibility of the pads in the MR images, (iii) ensure stable performances over time and (iv) limit impact on B_0 homogeneity. RF performances in terms of SAR and B_1^+ shimming have to be comparable to state-of-the-art barium titanate mixtures.

A novel mixture based on 4-Fluoro 1,3-dioxalan-2-one as a solvent and Polyethylene glycol as a dispersant and filled with Silicon carbide particles as a dielectric material is presented. We focused on a new solvent that shows a similar permittivity ε' to water, a fusion temperature slightly above 25°C and a high boiling temperature. These properties resulted in a more viscous matrix at ambient temperature to avoid particles sedimentation as well as reduced solvent evaporation. A dispersant was added according to its affinity with both the dielectric material and the solvent to ensure long-term homogeneity. Overall, the composition described lowers the safety concerns as the solvent safety information shows a toxicity rated as "skin irritant" (32). Meanwhile, the dielectric powder as well as the dispersant are rated as non-toxic (33, 34). The inhalation risk is reduced compared to the perovskite-based pads as the volatility of the solvent is very low at ambient temperature.

SiC pads are NMR invisible. This is due to both due to short T_2 (6.6 ms) and T_2^* (0.19 ms) relaxations time and to low proton density of the mixture. Therefore, it is expected that SiC pads should not be visible on most of standard MR sequences. Nevertheless, the short SiC T_2 and T_2^* can also be questioned with

regard to strong magnetic susceptibility effects. On one hand, short transversal relaxation time can be indeed related to a high magnetic susceptibility but on another hand, it can also be connected to the material structure (semi-solid). In case of strong magnetic susceptibility, major distortions should be seen on the images at the interface between pads and the head. Figure 4b and Figure 6 do not show any artifact either with $BaTiO_3$ nor with SiC. Literature reported similar behaviour for $BaTiO_3$ (9). Moreover, $BaTiO_3$ and SiC pads are identical in size and shape, the evidences confirm the hypothesis that the magnetic susceptibility of each mixture is comparable. Figure 5 demonstrates quantitatively that the presence of the dielectric pads affects weakly the static magnetic field and that standard B_0 shimming procedure was able to retrieve a good level of homogeneity. Our last objective of long-lasting performance was supported by relative permittivity measurements. We observe that the mixture can preserve its relative permittivity within a variation of 5% for the real part and 8% for the imaginary part after a one-year period. The variations obtained are within the accuracy of the measurement method. Recent tests using specific mixing machines over hand mixing suggest better mixture stability over time. On the other hand, mixture instability was reported for perovskite based dielectric pads. Several dispersant agents were studied to stabilize the composite performance. It was proven effective up to 6 months (14) but not longer. The RF performances were assessed on two different targets. On one hand, the SiC pads should not increase local SAR which is the main hurdle for UHF MRI (35). On the other hand, shimming performances should be comparable to barium titanate pads. Regarding local SAR study, we presented the SAR_{10g} maps in Figure 2 and a quantitative analysis in Table 1. We observed maximum local SAR was kept below the reference set by the transmit coil alone for each set of pads. Moreover, renormalizing the SAR values by B_1^+ amplitude in the middle of the brain which is similar to the RF calibration procedure in experiments, maximum local SAR for each set of pads remained smaller than the reference case with small variations on the order of a few percent. Based on these observations, we concluded that the SiC pads are as safe as the barium titanate pads in our configuration. Finally, we assessed the shimming efficiency of the pads with an in vivo study over four healthy volunteers under a restricted SAR protocol to ensure unconditional safety. We observed qualitatively the B_1^+ magnitude distribution

over the brain of volunteer #1 in Figure 4a. The median coronal slice showed significant improvements in the lower part of the temporal lobes. The transverse slice showed that low amplitude regions are still present for each set of pads and more pronounced on the left side of the SiC pads. These effects are attributed to disruptions from the pads magnetic field onto the circularly polarized magnetic field emitted by the birdcage. We can point out that a small asymmetry was already visible in the reference. The inhomogeneity in the temporal lobe on the left of the image was more pronounced for the SiC pads than the $BaTiO_3$ pads. Looking at performances combined over our cohort of four volunteers, we observed similar behaviour for each set of pads. Each set performed better on volunteer #1 (male) that had a larger head diameter and a more inhomogeneous distribution when the reference map was acquired. On average the SiC pads provided an B_1^+ amplitude enhancement of +25% in the temporal lobe ROIs with respect to the reference case. This enhancement was evaluated to be 3 to 4% less than with the $BaTiO_3$ pads. Simulation results had shown that the SiC case required more power to reach similar B_1^+ magnitude. This effect is due to higher losses in the SiC pads, having higher imaginary part of relative permittivity. We are convinced that it explains also the small gap between the SiC and $BaTiO_3$ pads performances observed experimentally. As shown in the MR images in Figure 4b and Figure 5, this gap affects partially the final MR images acquired. However, overall, the presence of the SiC pads improved the contrast of the images acquired in low and high resolution.

With the installation of the dielectric pads inside the coil, at a global brain level, B_1^+ NRMSE remained very high, 34% in average over transverse and coronal views for the 4 volunteers. Dielectric pads have mainly improved locally B_1^+ field in the temporal lobes (+25%), enough to bring back signal and contrast to noise to make the images readable in these regions (Figure 6). But such overall performances are way beyond what can be achieved with parallel transmission (pTx) system with suitable coil array and tailored multi-dimensional radiofrequency pulses B_1^+ NRMSE <7% or with Universal Pulses (UP self-calibrated RF pulses) with which B_1^+ NRMSE stayed <11% in average for MPRAGE sequence (36) and NRMSE <10% for newer UP pulse design and larger range of classic MR contrasts (37). Of course, this being said, the level of complexity and the budget are not at all in the same ranges. Also, to date, there is not a

pTx solution with tailored pulses for every single MR sequence required to achieve all relevant clinical protocols. Indeed, so far, this is a major limitation to the adoption of this solution at a large scale.

Conclusion

In conclusion, this work proposed a new dielectric material to be used in high dielectric constant pads. It is based on a low fusion temperature solvent combined with a safer dielectric powder. The new mixture presents several advantages compared to state-of-the-art BaTiO3 pads: reduced toxicity, invisibility in MR images and long-lasting performances. SiC pads were characterized for passive B_1^+ shimming to improve the signal contrast in the brain temporal lobes in a commercial 7T head coil. Results showed that performances in terms of SAR and B_1^+ shimming are close to state-of-the-art devices. We believe that this new pad composition will help to further establish the HDC pads as a user-friendly and safe strategy for reducing RF inhomogeneities and artifacts in UHF MRI.

Acknowledgements

This work has been supported by the Programme Transversal du CEA, the FET-OPEN M-CUBE Project (grant #736937), the FET-OPEN MRI PADS launchpad Project (grant #850506), the FET-PROACT M-ONE (project grant #952106), the Excellence Initiative of Aix-Marseille University - A*MIDEX, a french "Investissements d'Avenir" programme under Multiwave chair of Medical Imaging, the Leducq Foundation large equipment ERPT program, the NEUROVASC7T project, the Institut Carnot and the NSF/NIH/ANR program “Collaborative Research in Computational Neuroscience” (HIPLAY7, NSF-CRCSN-1607835 and ANR-16-NEUC-0001-01). The authors would like to thank Dr Alexis Amadon and Dr Bruno Pinho-Meneses for their help to acquire isotropic B_0 maps during the reviewing process.

References

1 - Meneses, B. P., and Amadon, A., A fieldmap-driven few-channel shim coil design for MRI of the human brain. Physics in Medicine & Biology 2021; 66.1: 015001.

2- Collins C.M., Liu W., Schreiber W., Yang Q.X., Smith M.B. Central Brightening Due to constructive Interference With, Without, and Despite Dielectric Resonance. J Magn Reson Imaging 2005; 21: 192-196

3- Yang Q.X., Wang J.H., Collins C.M., et al. Analysis of wave behaviour in dielectric sample at high field. Magn Reson Med 2002; 47: 982–989

4 - Van de Moortele, P. F., et al, B_1 Destructive Interferences and Spatial Phase Patterns at 7T with a Head Transceiver Array Coil, Magn. Reson. Med. 2005; 54: 1503-18.

5 - Webb, A.G., Dielectric materials in magnetic resonance. Concepts in Magnetic Resonance Part A. 2011; 38A(4): 148-84.

6 - Foo TK, Hayes CE, Kang YW. Reduction of RF penetration effects in high field imaging. Magn Reson Med 1992; 23(2): 287-301.

7 - Sunaga T, Ikehira H, Furukawa S, Tamura M, Yoshitome E, Obata T, et al. Development of a dielectric equivalent gel for better impedance matching for human skin. Bioelectromagnetics 2003; 24(3): 214-7.

8 - Takayama Y, Nonaka H, Nakajima M, Obata T, Ikehira H. Reduction of a high-field dielectric artifact with homemade gel. Magn Reson Med Sci 2008; 7(1): 37-41.

9 - Yang QX, Mao W, Wang J, Smith MB, Lei H, Zhang X, et al. Manipulation of image intensity distribution at 7.0 T: passive RF shimming and focusing with dielectric materials. J Magn Reson Imaging 2006; 24(1): 197-202.

10 - Yang QX, Wang J, Wang J, Collins CM, Wang C, Smith MB. Reducing SAR and enhancing cerebral signal-to-noise ratio with high permittivity padding at 3 T. Magn Reson Med 2011; 65(2): 358-62.

11 - Teeuwisse WM, Brink WM, Webb AG. Quantitative assessment of the effects of high-permittivity pads in 7 Tesla MRI of the brain. Magn Reson Med 2012; 67(5): 1285-93.

12 - Haines K, Smith NB, Webb AG. New high dielectric constant materials for tailoring the B_1^+ distribution at high magnetic fields. J Magn Reson. 2010; 203(2): 323-7.

13 - Neves AL, Leroi L, Raolison Z, Cochinaire N, Letertre T, Abdeddaïm R, et al. Compressed perovskite aqueous mixtures near their phase transitions show very high permittivities: New prospects for high-field MRI dielectric shimming. Magn Reson Med 2018; 79(3): 1753-65.

14 - Vaidya, M. V., et al. Improved detection of fMRI activation in the cerebellum at 7T with dielectric pads extending the imaging region of a commercial head coil. Journal of Magnetic Resonance Imaging 2018; 48.2: 431-440.

15 - Teeuwisse WM, Brink WM, Haines KN, Webb AG. Simulations of high permittivity materials for 7 T neuroimaging and evaluation of a new barium titanate-based dielectric. Magn Reson Med 2012; 67(4): 912-8.

16 - O'Reilly TPA, Webb AG, Brink WM. Practical improvements in the design of high permittivity pads for dielectric shimming in neuroimaging at 7T. J Magn Reson 2016; 270: 108-14.

17 - Calcium Titanate Oxide: MSDS No. 11397. Alfa Aesar website. Accessed Nov, 2021.

18 - Barium Titanate Oxide: MSDS No. 12348. Alfa Aesar website. Accessed Nov 2021.

19 - Fagan, A. J., et al. Image Artifact Management for Clinical Magnetic Resonance Imaging on a 7 T Scanner Using Single-Channel Radiofrequency Transmit Mode. Investigative radiology 2019;54.12: 781-791.

20- Raolison Z, Dubois M, Neves AL, Enoch S, Mallejac N, Sabouroux P, et al. Properties optimization of pads configurations on CST, Proceedings of the International Society for Magnetic Resonance in Medicine, Paris, France; 2018.

21- van Gemert J, Brink W, Webb A, Remis R. High-permittivity pad design tool for 7T neuroimaging and 3T body imaging. Magn Reson Med. 2019;81:3370–3378

22- Raolison Z, Abdeddaïm R, Leroi L, Neves AL, Dubois M, Mauconduit F, Luong M, Enoch S, Mallejac N, Sabouroux P, et al. Evaluation of a new long-lasting silicon carbide based dielectric pad for ultra-high field MRI. Proceedings of the International Society for Magnetic Resonance in Medicine, Paris, France; 2018.

23- Simpkin R. Derivation of Lichtenecker's Logarithmic Mixture Formula From Maxwell's Equations. IEEE Transactions on Microwave Theory and Techniques 2010;58(3):545 50.

24 - Nicolson AM, Ross GF. Measurement of the Intrinsic Properties of Materials by Time-Domain Techniques. IEEE Transactions on Instrumentation and Measurement 1970;19(4):377-82.

25 - Georget E, Abdeddaim R, Sabouroux P. A quasi-universal method to measure the electromagnetic characteristics of usual materials in the microwave range. Comptes Rendus Physique 2014;15(5):448-57.

26 - Wolf, S., et al. SAR simulations for high-field MRI: How much detail, effort, and accuracy is needed? Magnetic resonance in medicine 69.4; 2013: 1157-1168.

27 - International Electrotechnical Commission. Medical electrical equipment - Part 2–33: particular requirements for the safety of magnetic resonance diagnostic devices. EC 60601-2-33. 3.0; 2010.

28 - Vignaud A, Mauconduit F, Gras V, Girard O, Kober F, Hertz-Pannier L, et al. Fast and unconditionally safe in vivo MR head protocol for home-made coil prototype assessment at 7T. Proceedings of the ESMRMB. Rotterdam, Netherlands; 2019.

29 - Marrakchi-Kacem, L., et al Robust imaging of hippocampal inner structure at 7T: in vivo acquisition protocol and methodological choices. MAGMA 2016; 29:475-89

30 - Schmidt R, Slobozhanyuk A, Belov P, Webb AG. Flexible and compact hybrid metasurfaces for enhanced ultra-high field in vivo magnetic resonance imaging. Sci Rep 2017;7(1):1678.

31 - Schmidt R, Webb A. Improvements in RF Shimming in High Field MRI Using High Permittivity Materials With Low Order Pre-Fractal Geometries. IEEE Trans Med Imaging 2016;35(8):1837-44.

32 - Fluoroethylene carbonate: MSDS No. 3205E-3. Kishida chemicals website. Accessed Nov 2021.

33 - Silicon carbide: MSDS No. 357391. Sigma Aldrich website. Accessed Nov 2021.

34 - Polyethylene Glycol: CAS 25322-68-3. ThermoFisher. Revised April 25, 2019.

35 - Collins CM, Li S, Smith MB. SAR and B_1 field distributions in a heterogeneous human head model within a birdcage coil. Specific energy absorption rate. Magn Reson Med 1998; 40:847–856.

36- Gras V, Vignaud A, Amadon A, Le Bihan D, Boulant N. Universal pulses: A new concept for calibration-free parallel transmission. Magn Reson Med 2017; 77: 635-643

37- Van Damme L, Mauconduit F, Chambrion T, Boulant N, Gras V. Universal nonselective excitation and refocusing pulses with improved robustness to off-resonance for Magnetic Resonance Imaging at 7 Tesla with parallel transmission. Magn Reson Med 2021; 85: 678-693.